A PROPOSED CONTROL STRATEGY TO IMPROVE THE LOW VOLTAGE RIDE THROUGH CAPABILITY OF PV SYSTEM WITH KEEPING THE DC-LINK VOLTAGE CONSTANT

Ebrahim A. BADRAN (ebadran@hotmail.com), **Khaled M. ABO-AL-EZ**(ezzkhalid@mans.edu.eg), and **Haider MUAELOU** (haidar_alqurashy@yahoo.com)
Faculty of Engineering, Mansoura University, Egypt

Abstract: *In modern electric power systems, the dependence on solar power is increasing. The grid connected applications are very important with the deficit in conventional power stations due to fuel shortage. This paper focuses on controller design and implementation in grid connected PV systems for low voltage rid through (LVRT) in distribution power systems, this paper proposes a control method to keep the dc-link voltage of PV system constant during low voltage rid through (LVRT). This is done by changing the operating point on the I/V curve of the PV cell from the MPPT point to another point, the active power output of the PV will decrease from the maximum to the needed value. The proposed control system is evaluated under different fault scenarios to test the validity of the control system. The results show that the proposed control system gives the expected performance. The PSCAD package is used for simulating this study.*

Keywords: *Control system, Photovoltaic systems, Low-voltage-ride-through, Distribution system, PSCAD*

1. Introduction

In recent years, more efforts have been made on the integration of PV systems into the grid in order to meet the imperative demand of a clean and reliable electricity generation. Electric power generation through solar energy process is one of the more methods available at the moment, during the operation of solar energy systems do not generate any greenhouse gas pollution of the environment [1]. The high penetration of PV energy into the power system has resulted in power system operators revising the grid codes requirements for interconnection of this type of generation. A special focus in these requirements is drawn to the PV fault ride-through capability (LVRT), which addressed primarily the design of the PV controller in such that PV is able to remain connected to the network during abnormal operation condition as well as can contribute to voltage support during and after the abnormal operation conditions. LVRT capability is defined as the PV system should stay connected to the grid in the event of grid failures and injects reactive power to help the grid during the grid fault [2]. There are many researches dealt with the performance of grid-connected PV system under various fault conditions. In [3], the high penetration of PV have affect on the reactive power supplied by the PV plant. During the fault, the control strategy makes the PV system is capable ride the drop voltage and support the grid by injecting the reactive current. As a result to inverter limit, the active current will decrease to avoid over current. The unbalanced power between grid side and PV side causes increasing of the DC-Link capacitor voltage which causes semiconductor devices damage [4]. Also, the excessive of DC voltage and excessive AC currents causing inverter disconnection [5]. To maintain the DC-link voltage constant, dc-chopper circuit between the inverter and the DC-Link is used in [6] to absorb the power at DC side and to maintain the power balance. In [7], the performance of LVRT control strategy is improved by using the super capacitor at the DC side. The super capacitor is used to absorb extra input power or to compensate the shortage of the output power. Nowadays, PV control strategies are developed in order to reader that the PV system acquires LVRT capability when the faults occur in the grid [8]. The super capacitor can coordinate with the PV system internal power at normal operation. At fault mode, the super capacitor absorbs energy at the DC side and balances the power to avoid changes to DC bus voltage [8]. Unfortunately using the dc-chopper circuit and the super capacitor as a hardware protection for DC-Link capacitor increases the cost. In this paper, LVRT of PV in distribution power systems with keeping the DC link voltage to be constant by internal control is achieved. Three LVRT techniques for the PV are simulated and compared.

2. Grid codes

During the fault, it is required from the PV system to supply a reactive current to enhance the grid stability based on the grid code of the PV system. Fig. 1 illustrates the low voltage ride-through requirement of E.ON grid code for PV system [9]. In addition Fig. 2 shows the relationship between the increment of reactive current and the voltage drop.

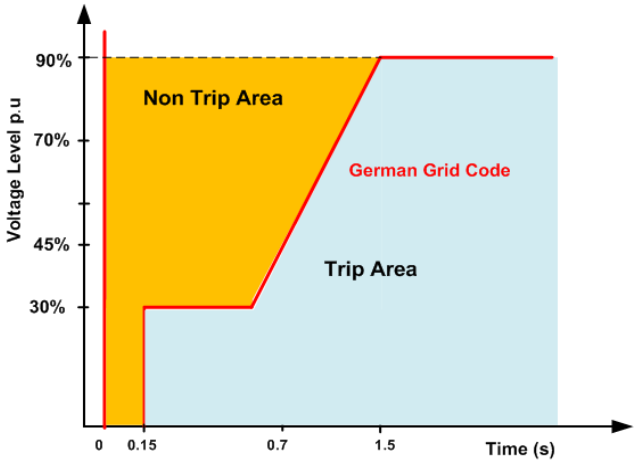

Fig. 1. LVRT requirement for PV system of E.ON [9].

For the E.ON as shown in Fig. 1. the PV inverter should stay connected to the grid when the voltage drops to 0 V for 0.15 seconds and inject some reactive current into the grid. Fig. 2 shows the grid requirement and the relationship between the voltage drop and injected reactive current.

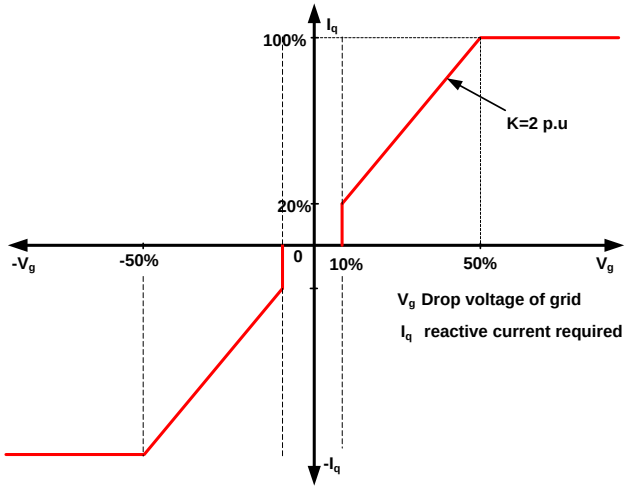

Fig. 2. Voltage support requirement under grid fault for PV system [9].

3. Modeling of grid-tied PV system

The overall model of grid-tied PV system is shown in Fig. 3 including a PV source, a DC-link capacitor for minimizes the voltage ripple across the PV terminals, a DC-DC converter, a DC-DC controller with maximum power point tracking (MPPT), the grid interface inverter for convert the DC output power of the PV system to a three phase AC power through Pulse Width Modulation (PWM), using Insulated-Gate Bipolar Transistors switches (IGBTs), an appropriate inductance filter to remove the high order harmonics from the voltage and the current of the inverter, and step up transformer with wye grounded winding connection type at the inverter side and delta winding at the grid side.

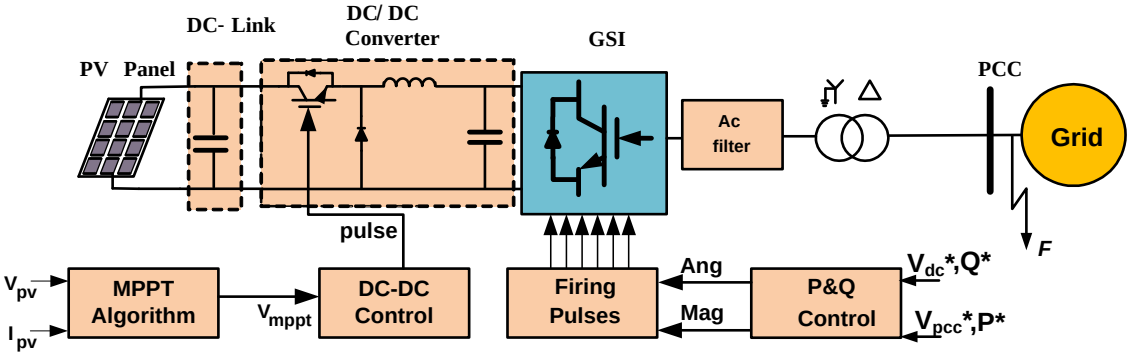

Fig. 3. Grid-tied PV model.

3.1. PV source model

The solar cell is a semiconductor device that converts the solar radiation directly to electrical energy, with no pollutant emission. The output from a single cell is not suitable for practical cases. To obtain sufficient voltage the cells are connected in series. To obtain sufficient current, they are connected in parallel to form a PV module. The modules can be also connected in series and in parallel to form a PV array with the required rated power [10],[11]. In this paper, a 150 kW PV system is investigated. The equivalent electrical circuit of a PV cell which contains a current source anti-parallel with a diode, a shunt resistance, and a series resistance as shown in Fig. 4 [11],[12].

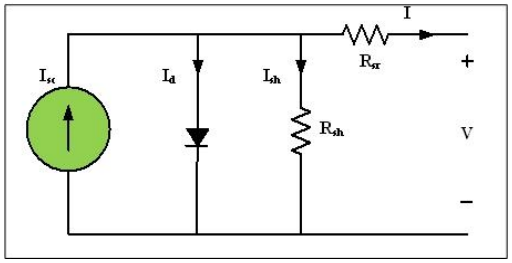

Fig. 4. The PV cell equivalent circuit.

The basic equation that characterizes the solar cell I/V relationship can be derived after apply Kirchhoff's current law on PV cell equivalent circuit as;

$$I = I_{sc} - I_d - I_{sh} \quad (1)$$

After compensation diode equation current I_d and current parallel branch I_{sh} equation (1) becomes as [1];

$$I = I_{sc} - I_o \left[\exp\left(\frac{V+IR_{sr}}{nkT_c/q}\right) - 1\right] - \left(\frac{V+IR_{sr}}{R_{sh}}\right) \quad (2)$$

I_{sc} is the short circuit current and it is a function of the solar radiation on the plane of the solar cell G and the cell temperature T_c, as given by;

$$I_{sc} = I_{scR} \frac{G}{G_R}[1 + \alpha_T (T_c - T_{cR})] \quad (3)$$

The current I_o in equation (2) is called the dark current. It is a function of cell temperature only, and is given by;

$$I_o = I_{oR} \left(\frac{T_c^3}{T_{cR}^3}\right) \exp\left[\left(\frac{1}{T_{cR}} - \frac{1}{T_c}\right)\frac{qe_g}{nk}\right] \quad (4)$$

where I_{scR} is the short circuit current at the reference solar radiation G_R and the reference cell temperature T_{cR}. The parameter αT is the temperature coefficient of photo current, I_{oR} is the dark current at the reference temperature, q is the electron charge, k is the Boltzmann constant, e_g is the band gap energy of the solar cell material, and n is the diode ideality factor. The constants of the above equations are set by the manufacturers.

3.2. DC -DC converter

It is known that the efficiency of the solar PV module is low (about 13%). Therefore, it is desirable to operate the module at the peak power point in order to maximize the delivered power to the load under varying temperature and solar radiation conditions. Hence, maximization of power improves the utilization of the solar PV module. The dc-dc converter serves the purpose of transferring maximum power from the PV module to the load by changing the duty cycle. The load impedance as seen by the source is varied and matched at the point of the peak power with the source. So, the maximum power is transferred. In this paper, the step down converter is used, which consists of a power switch that is followed by an inductor, a diode and output capacitance [11],[13], as shown in Fig. 5.

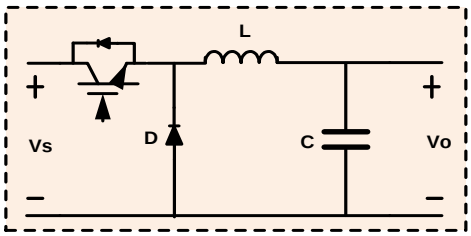

Fig. 5. DC -DC step down converter model.

3.3. DC-DC converter controller with (MPPT)

The relationship between current and voltage of the PV cell is non-linear. There is an unrivaled point on the I/V curve, called the Maximum Power Point (MPP), at which the entire PV system operates with maximum efficiency and gives its maximum output power. The location of the MPP is not known, but it can be determined, either through calculation models or by search algorithms in order to maintain the PV array's operating point at its MPP.

The optimum operating point of solar cells occurs at the knee of the I/V curve. In this paper the incremental conductance algorithm is used. This method tracks the peak power under fast varying atmospheric condition. In this method the derivative of PV output power with respect to its output voltage is calculated (dP/dV). When dP/dV approaches zero the maximum PV output power can be achieved [11],[14]. The controller calculates dP/dV based on the measured PV incremental output power and voltage. If dP/dV is not close to zero, the controller

will adjust the PV voltage step by step until dP/dV approaches zero, at which the PV array reaches its maximum output.

The mathematical description of this method is illustrated using;

$$P = V\,I \quad (5)$$

With incremental change in current and voltage, the modified power is given by [11],[15];

$$P+\Delta P = (I+\Delta I).(V+\Delta V) \quad (6)$$

After ignoring small terms, equation (6) is simplified to;

$$\Delta P = \Delta V.I + \Delta I.V \quad (7)$$

ΔP must be zero at peak point. Therefore, at peak point equation (7) becomes;

$$dI/dV = -I/V \quad (8)$$

The incremental algorithm is based on the following equation holds at the MPP [14]:

$$dI/dV + (I/V) = 0 \quad (9)$$

3.4. Control of inverter without LVRT

The inverter control system of PV uses two PI controllers [16]. The PI controller is most widely and commonly used controller in the process industry because the number of parameter to adjust in PI controller is very small and many tuning methods and algorithms are available that can be implemented for parameter adjustment [5],[17],[18]. The features of PI controller are: The proportional term (k) immediately impacts controller bias or null value based on the size of the error signal at a particular time, also the past history and current trajectory of the controller error have no influence on the proportional term computation. The integral term (t) continually sums up error, through constant summing integral action accumulates influence based on how long and how far the measured process variable has been from set point over time. The first PI controller controls the active power (P) of PV by adjusting the DC bus voltage between the DC-DC converter and the inverter. The active power control model is shown in Fig. 6 [16]. The second PI controller controls the reactive power (Q) to be zero. The reactive power control model is shown in Fig. 7 [16]. The output of the controllers Angle and Magnitude will be also used as an input to the firing pulse generator of the inverter using PWM control technique.

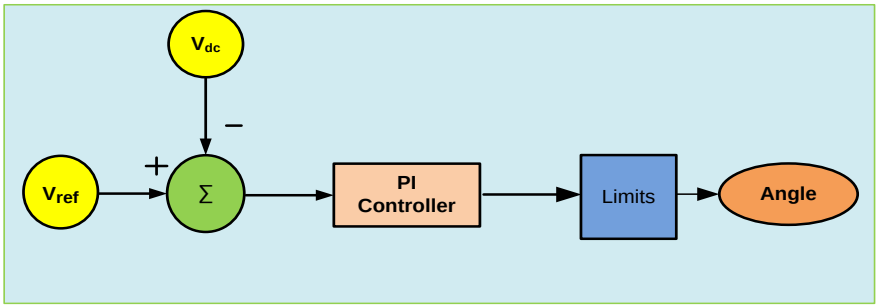

Fig. 6. The active power control model.

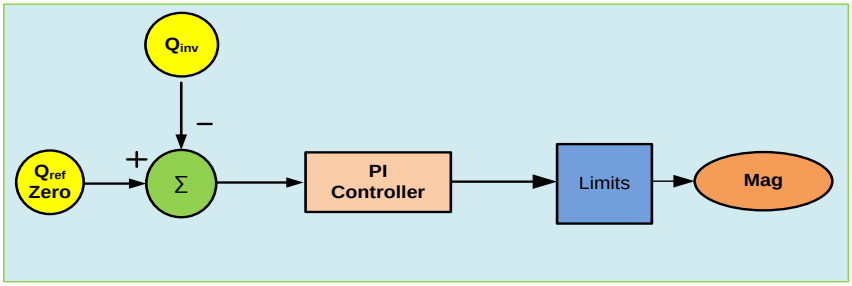

Fig. 7. The reactive power control model.

4. LVRT control strategy of the PV system

The proposed LVRT control strategy of the PV system which is used in this paper consists of two parts**.** The first part controls the active power and consists of two PI controllers; one for normal operation mode and the other for fault mode. The second part controls the reactive power and consists of two PI controllers, one for normal operation mode and the other for fault mode. Fig. 8 shows the proposed LVRT control system. In this paper the parameters of PI controllers of active and reactive power are determined using try and error method [19].

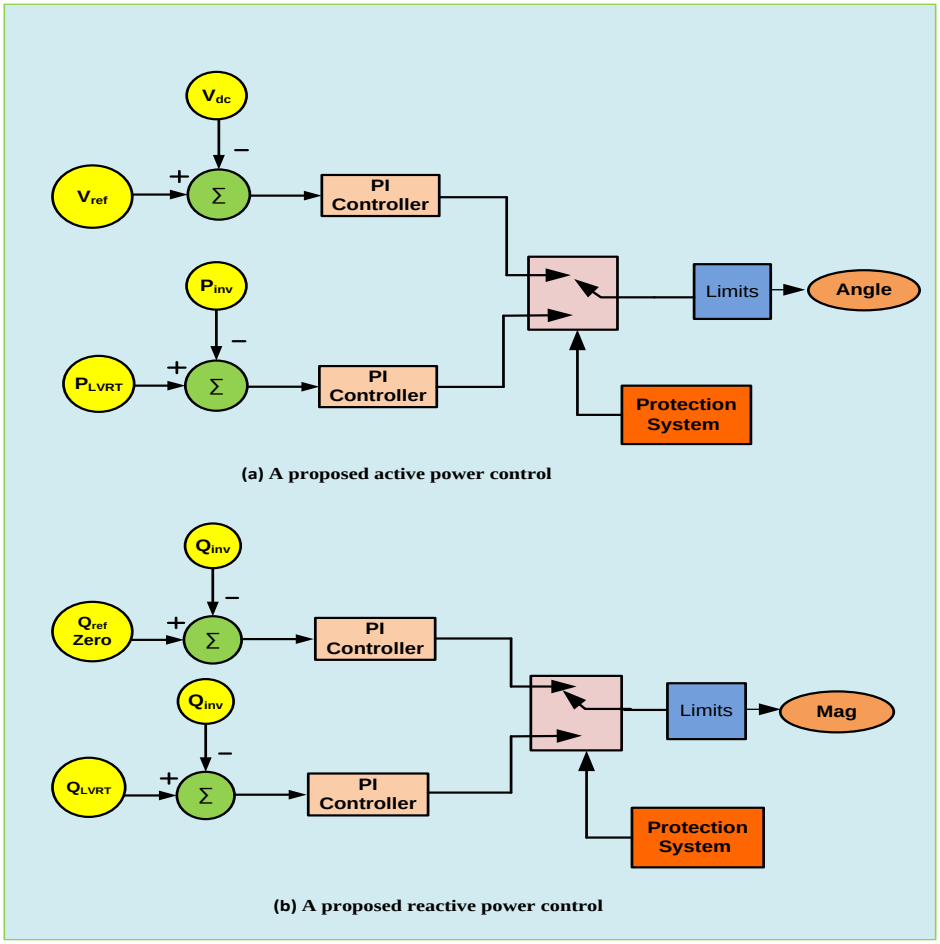

Fig. 8. The proposed LVRT control

The model has stable responses at steady state and fault conditions. The proportional and integral gains of each PI controller are listed in Table 1.

Table 1. Different PI controllers parameters.

Different PIs / Mode	Active Power PI Controller	Reactive Power PI Controller
Normal Mode	k_1=20 t_1 =0.06	k_2=3 t_2 =0.01
Fault Mode	k_3=7 t_3 =0.004	k_4=0.007 t_4 =0.006

When the fault occur, the protection system detects the fault and transfers the control mode from the normal mode operation to the LVRT mode. Through the LVRT mode, the control system of the PV will operate with new active and reactive power reference values. These reference values can be calculated using equations (10)-(12) which are listed in [20] under LVRT requirements of PV system. The LVRT requirements state that the PV must inject reactive power to the grid in order to support grid voltage during the grid fault without exceeding the PV inverter rating. The amplitude of the injected reactive current , I_Q, must not exceed the maximum inverter current , I_{max} , to protect the inverter from over load as listed in equations (13) and (14) [20]. The overall LVRT scheme used for determining the active and reactive power reference values is shown in Fig. 9 [20].

$$P = \sqrt{3}.VI_P \quad (10)$$

$$Q = \sqrt{3}.VI_Q \quad (11)$$

$$I_Q = \frac{V_n - V_{min}}{V_n} \times K\ 100\% \quad (12)$$

$$I_{max} = \sqrt{{I_P}^2 + {I_Q}^2} \quad (13)$$

$$I_P = \sqrt{{I_{max}}^2 - {I_Q}^2} \qquad (14)$$

where I_P is the active current, I_Q is the reactive current, V_n is the nominal voltage in pu , V_{min} is the minimum voltage drop during the fault and K=2.

The grid voltage is measured and compared with the nominal voltage then the difference between the two value is divided by the nominal voltage to get the percentage voltage drop during the voltage. The percentage voltage drop is multiplied by factor (K) which is defined by the grid code to get the reference reactive current that should be injected to the grid according to the grid code.

The reactive power reference is then calculated using equation (11) in pu and then multiplied by the PV rating (VA) (S rated). The reference active current (I_P) can be calculated using equation (14). The new reference active power is then calculated using equation (10) in pu and then multiplied by the PV rating (VA) (S rated) to get the value in Volt Ampere.

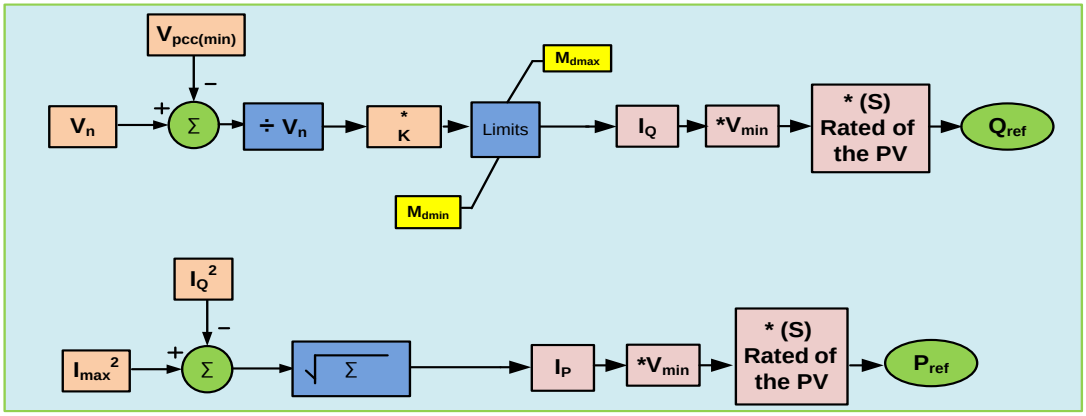

Fig. 9. The LVRT reference of active and reactive power calculation

During the fault the PV system decreases the injected active power to the grid in order to be able to inject reactive power according to grid code without exceeding the PV inverter rating. The DC-Link voltage increases due to the power imbalance between the injected active power to the grid and the PV side power which may damage the semiconductor devices. To protect the DC-link capacitor and the semiconductor devices a DC-chopper is used as a protection circuit to keep the DC-link voltage constant during the fault [6]. In this paper, a DC-link voltage control system is proposed to keep the DC-link voltage constant during the fault without using a DC-chopper. The proposed DC-link voltage control system is shown in Fig. 10. It consists of two operating modes. The first one is the normal operation mode. The objective of this mode is to extract the maximum power from the PV system by operating at a maximum power point. The second is the fault condition mode. The objective of this mode is to make the PV system generates active power equal to the active power injected to the grid in order to keep power balance at the two sides of the DC-link and meanwhile keeps the DC-link voltage constant.

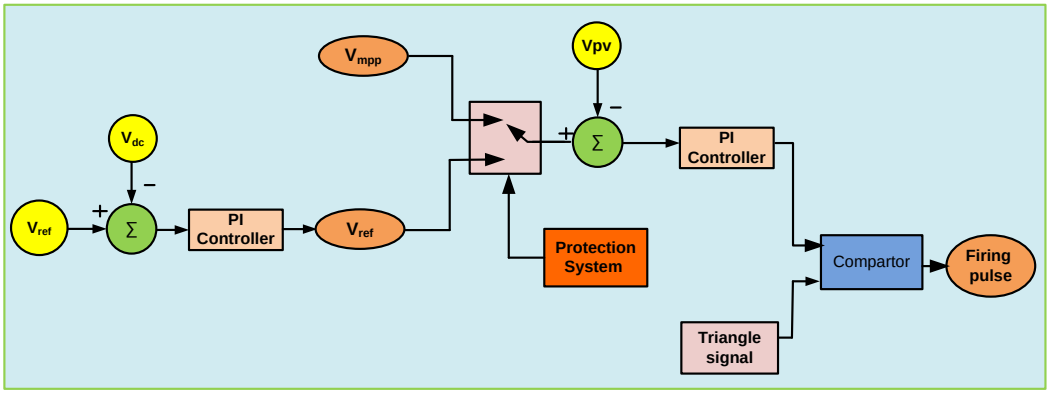

Fig. 10. The proposed for DC-link voltage control system

5. Simulation results

The PV system is tested and evaluated with three different control strategies the first control strategy used the active and reactive power control model as shown in Fig. 8, And the reference values of active and reactive power can be calculated using equation from (10) to (14) as illustrated in Fig. 9. Then the PV system is tested and evaluated with the second control strategy which is similar to the first control strategy but with additional DC-chopper circuit as a hardware protection. Finally the PV system is tested with the third proposed control strategy in which the active and reactive power is controlled using control models in Fig. 8 and Fig. 9 but with additional DC-link voltage control system which controls the DC power output of the PV as shown in Fig. 10. The PV system is tested under the following scenarios:

5.1 Three phase to ground fault at F in Fig. 4 with the first control strategy, and at drop voltage 50%.
5.2 Three phase to ground fault at F with the second control strategy, and at drop voltage 50%.
5.3 Three phase to ground fault at F with a proposed DC-link voltage control system, and at drop voltage 50%.
5.4 Double line to ground fault at F with a proposed DC-link voltage control system, and at drop voltage 50%.
5.5 Single line to ground fault at F with a proposed DC-link voltage control system, and at drop voltage 50%.
5.6 Three phase to ground fault at F with a proposed DC-link voltage control system, and at drop voltage 30%.
5.7 Three phase to ground fault at F with a proposed DC-link voltage control system, and at drop voltage 70%.
5.8 Three phase fault to ground at F with a proposed DC-link voltage control system, and at drop voltage to zero.

5.1The performance without DC-Link protection

The performance of the PV with the first control strategy under a three phase to ground fault with a voltage dip of 50 % for 0.4 sec is shown in Fig. 11. It is found from the simulation results that the active power injected to the grid is reduced to zero pu while, the PV active power at DC side remains constant at 1 pu, then the DC-Link voltage increases to 1.4 pu due to unbalance power, that can damage both the DC-Link capacitor and the semiconductor devices. The PV injects reactive power of 0.5 pu into the grid according to the grid codes and the inverter current is within the inverter current limits. The PV active current injected to the grid is reduced to zero pu but the PV reactive current injected to the grid is 1 pu.

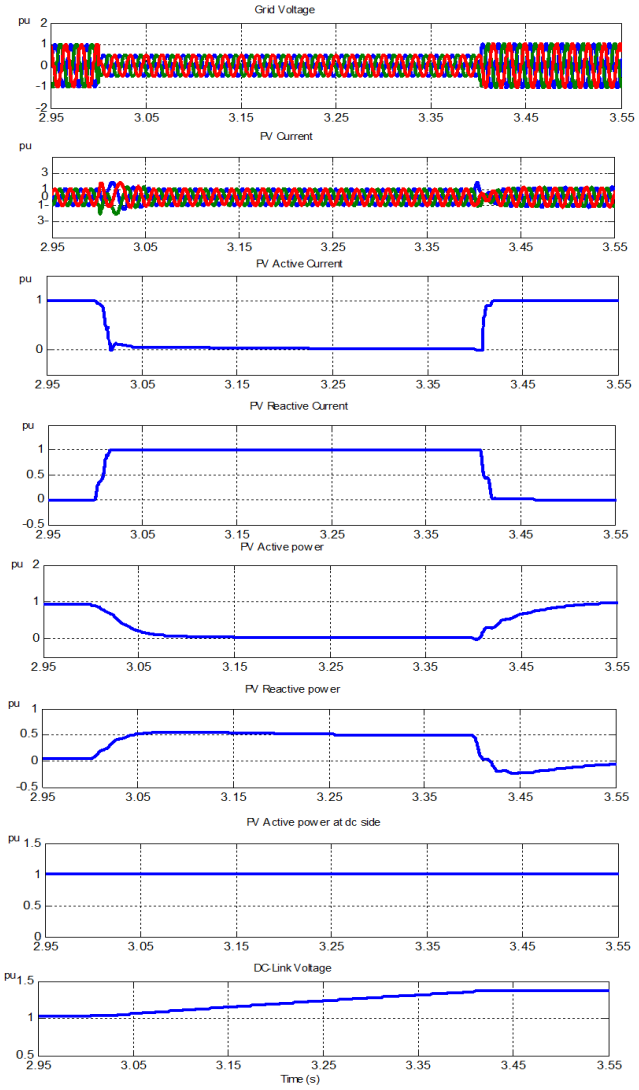

Fig. 11. Performance of the PV system at three phase to ground fault, 50% voltage dip for 0.4 sec at t=3 sec, without DC-link protection system.

5.2The Performance with DC-Chopper protection

The performance of the PV with second control strategy under a three phase to ground fault with a voltage dip of 50 % for 0.4 sec is shown in Fig. 12. It is found from the simulation results that the active power injected to the grid is reduced to zero in order to allow injecting reactive power of 0.5 pu to the grid while, the PV active power at DC side remains constant as 1 pu, but it is absorbed by the DC-Chopper resistance, then the DC-Link voltage is constant at 1 pu. The inverter current is within the inverter current limits. The PV active current injected

to the grid is reduced to zero pu but the PV reactive current injected to the grid is 1 pu.

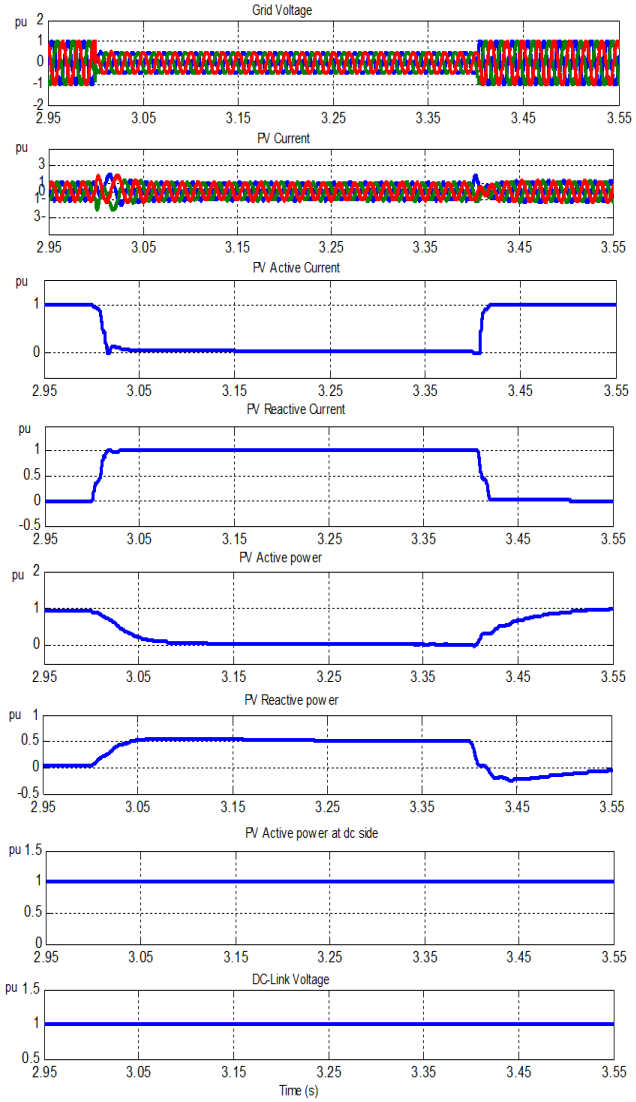

Fig. 12. PV performance at three phase fault, 50% voltage dip for 0.4 sec at t=3 sec with dc-chopper hardware protection system

5.3 The Performance with a proposed DC-link voltage control system

The performance of the PV with a proposed DC-link voltage control system under a three phase to ground fault with a voltage dip of 50 % for 0.4 sec is shown in Fig. 13. It is found from the simulation results that the active power injected to the grid is reduced to zero pu in order to allow injecting reactive power of 0.5 pu to the grid. The PV active power at DC side is reduced to zero pu in order to achieve active power balance at the two sides of the DC-Link, then the DC-Link voltage is constant at 1 pu. The inverter current is within the inverter current limits. The PV active current injected to the grid is reduced to zero pu but the PV reactive current injected to the grid is 1 pu.

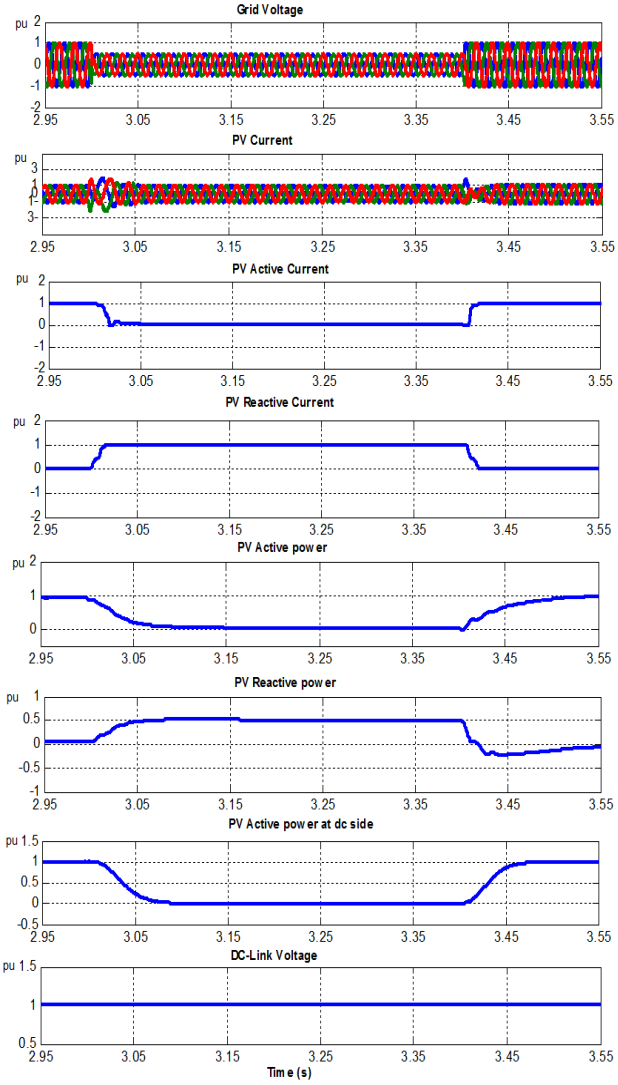

Fig. 13. PV performance at three phase fault, 50% voltage dip for 0.4 sec at t=3 sec with a proposed DC-link voltage control system

5.4 The Performance with a proposed DC-link voltage control system

The Performance of the PV with a proposed DC-link voltage control system under double line to ground fault with a voltage dip of 50 % for 0.4 sec is shown in Fig. 14. It is found from the simulation results that the active power injected to the grid is reduced to zero pu in order to allow injecting reactive power of 0.5 pu to the grid. The PV side active power is reduced to zero pu in order to achieve active power balance, then the DC-Link voltage constant as 1 pu. The inverter current is within the inverter current limits. The PV active current injected to the grid is reduced to zero pu but the PV reactive current injected to the grid is 1 pu.

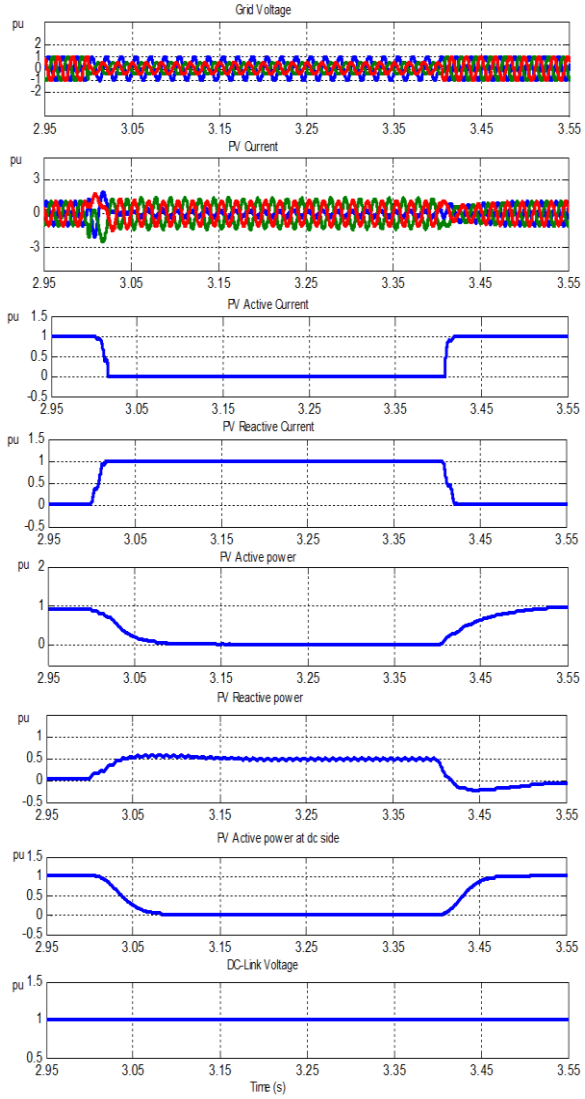

Fig. 14. PV performance at 2LG fault, 50% voltage dip for 0.4 sec at t=3 sec with a proposed DC-link voltage control system

5.5 The Performance with a proposed DC-link voltage control system

The Performance of the PV with a proposed DC-link voltage control system under single line to ground faults with a voltage dip of 50 % for 0.4 sec is shown in Fig. 15. It is found from the simulation results that the active power injected to the grid is reduced to zero pu in order to allow injecting reactive power approximately of 0.5 pu to the grid. The PV side active power is reduced to zero pu in order to achieve active power balance, then the DC-Link voltage constant as 1 pu. The inverter current is also within the inverter current limits. The PV active current injected to the grid is reduced to zero pu but the PV reactive current injected to the grid is 1 pu.

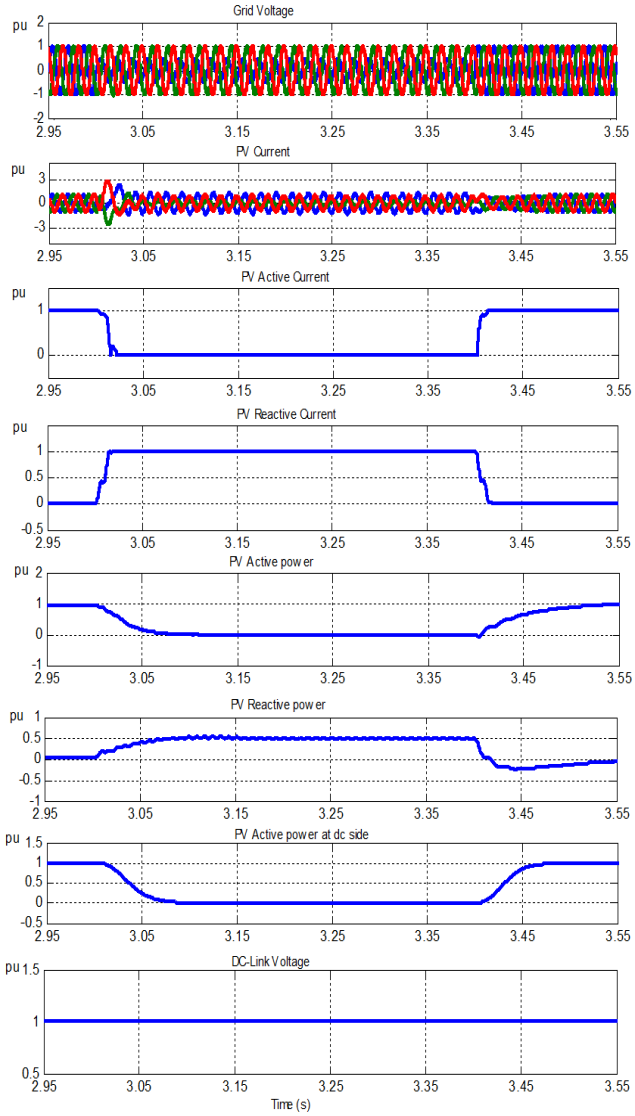

Fig. 15. PV performance at single line to ground fault, 50% voltage dip for 0.4 sec at t=3 sec with a proposed DC-link voltage control system

5.6 The Performance with a proposed DC-link voltage control system

The performance of the PV with a proposed DC-link voltage control system under a three phase to ground fault with a voltage dip of 30 % for 0.4 sec is shown in Fig. 16. It is found from the simulation results that the active power injected to the grid is reduced to 0.56 pu in order to allow injecting reactive power of 0.42 pu to the grid. The PV active power at DC side is reduced to 0.56 pu in order to achieve active power balance, then the DC-Link voltage constant as 1 pu. The inverter current is within the inverter current limits. The PV active current injected to the grid is 0.8 pu but the PV reactive current injected to the grid is 0.6 pu.

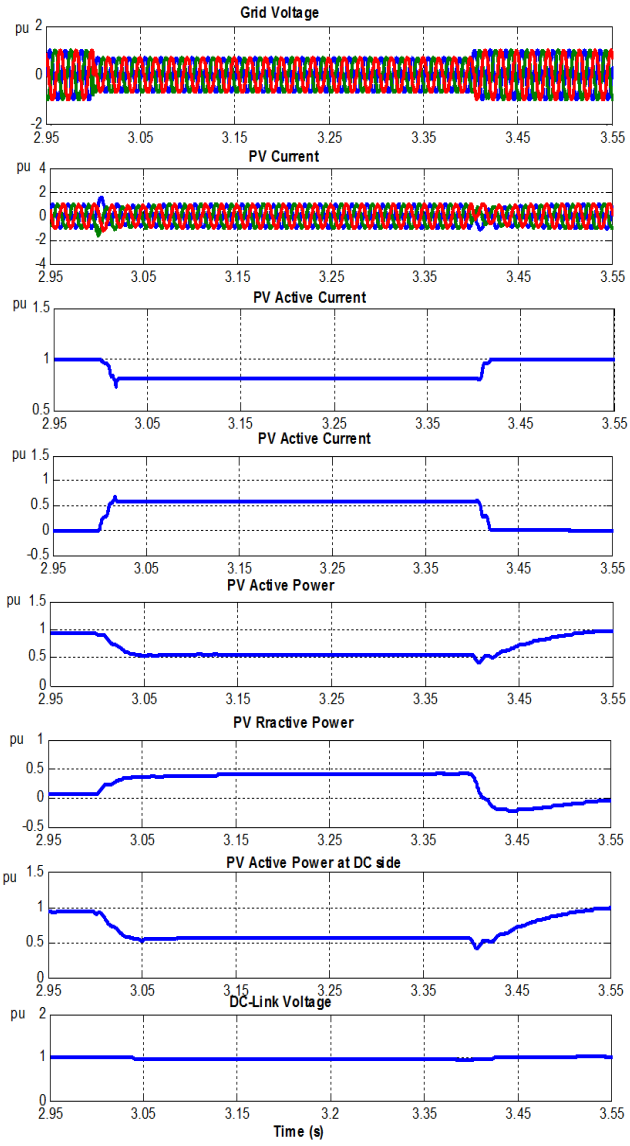

Fig. 16. PV performance at three phase to ground fault, 30% voltage dip for 0.4 sec at t=3 sec with a proposed DC-link voltage control system

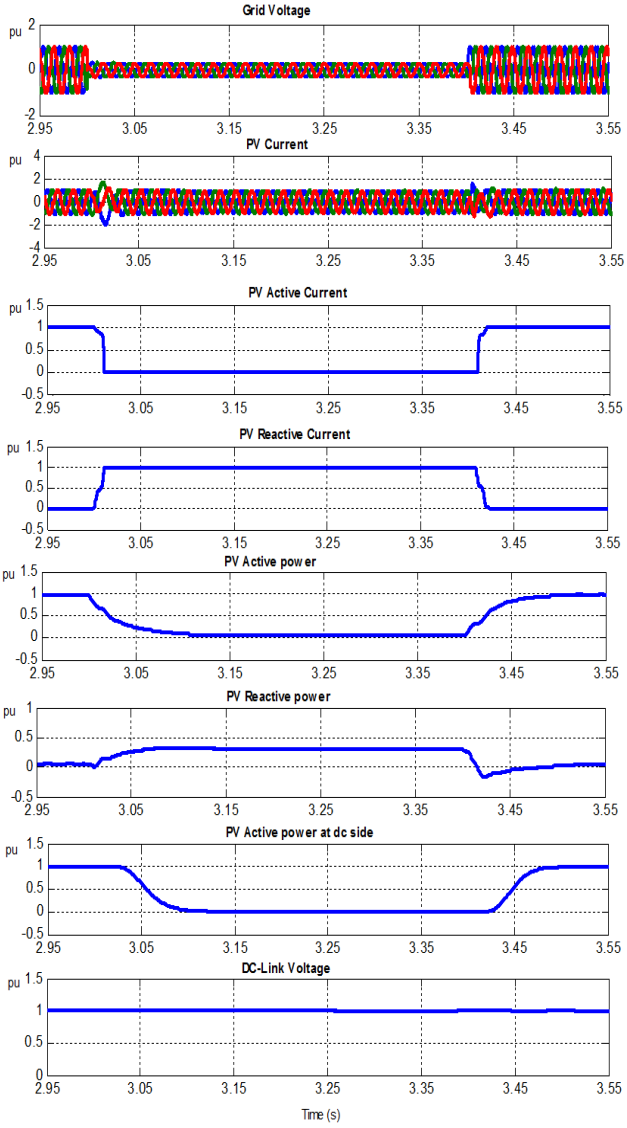

Fig. 17. PV performance at three phase to ground fault, 70% voltage dip for 0.4 sec at t=3 sec with a proposed DC-link voltage control system

6.7 The Performance with a proposed DC-link voltage control system

The performance of the PV with a proposed DC-link voltage control system under a three phase fault with a voltage dip of 70 % for 0.4 sec is shown in Fig. 17. It is found from the simulation results that the active power injected to the grid is reduced to zero pu in order to allow injecting reactive power of 0.3 pu to the grid. The PV active power at DC side is reduced to zero pu in order to achieve active power balance, then the DC-Link voltage constant as 1 pu. The inverter current is within the inverter current limits. The PV active current injected to the grid is 0 pu but the PV reactive current injected to the grid is 1 pu.

5.8 The performance with a proposed DC-link voltage control system

It is found from the simulation results that The PV system should stay connect into grid for 0.15 second according to grid code. Then, the PV system is disconnected from the grid due to the voltage drop time is exceeds the maximum allowed LVRT delay time i.e. the fault voltage drop profile is located outside the non-trip area of the LVRT curve shown in Fig. 1, during the fault the PV achieve the LVRT requirements by injecting reactive power of 0.15 pu to the grid. The active power is reduced to 0 pu in order to allow injecting reactive without exceeding maximum inverter current. The inverter current is also within inverter current limits. The PV active

current injected to the grid is 0 pu but the PV reactive current injected to the grid is 1 pu. After PV disconnection the active and reactive power are reduced to zero.

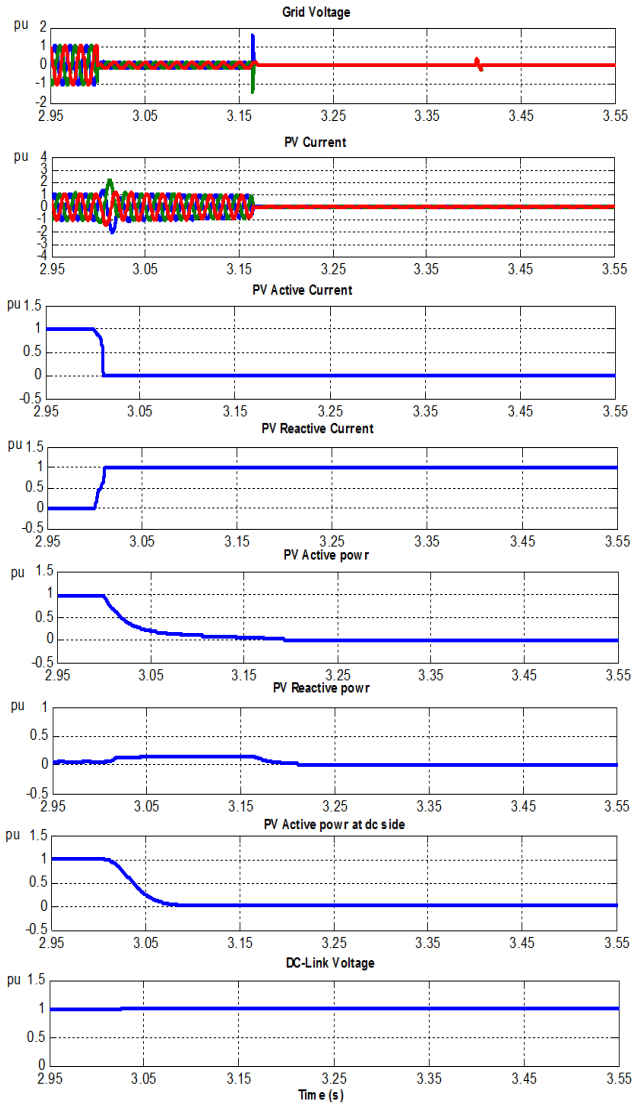

Fig. 18. PV performance at three phase to ground fault with voltage drop 85% for 0.4 second

6. The operation flow chart of the PV

The operation flow chart of the PV system under different modes of operation including the proposed control strategy is shown in Fig. 19.

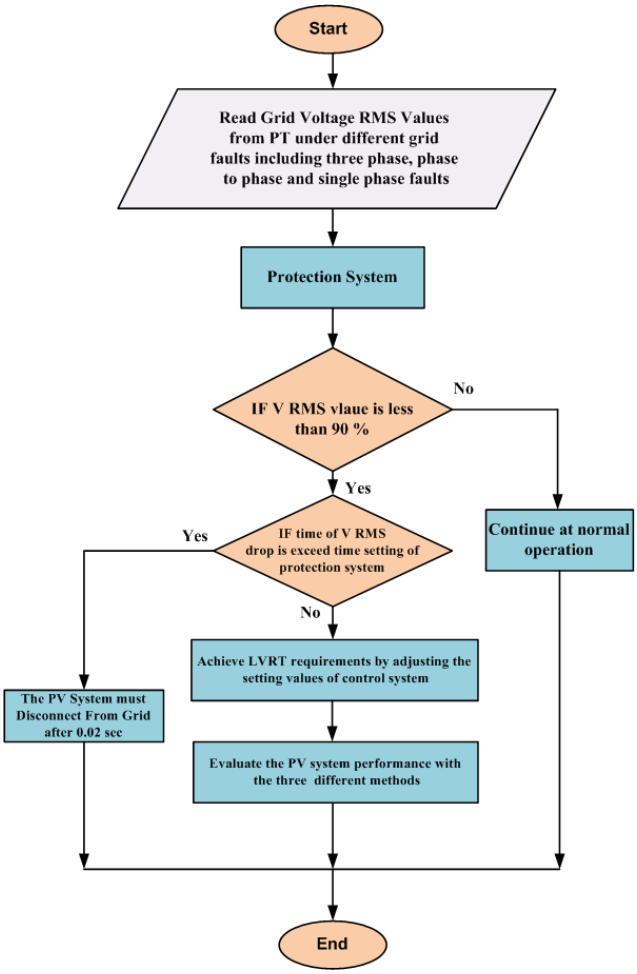

Fig. 19. The operation flow chart of the PV system with the proposed control

7. CONCLUSIONS

In this paper, a proposed control strategy of grid connected PV systems for LVRT capability in distribution power systems with a proposed DC-link voltage control system is presented. The proposed control enables the PV system to generate a reactive power during fault to support the grid. This helps the grid to maintain voltage stability during fault. Also, the PV system can supply the reactive power during fault without using a DC-Chopper as a hardware protection to keep the DC-Link voltage constant. This lead to a reduction in the total cost of the PV system. The proposed system is tested under different test cases, It is found that the PV system with the proposed control system has the capability of LVRT.

Appendix

A detailed discussion about the parameters of PV cell and PV array, are set as shown in Table 2 and Table 3.

Table 2. PV Cell Parameters

1	Effective area / cell (m^2)	0.01
2	Series resistance / cell (Ω)	0.02
3	Shunt resistance / cell (Ω)	1000
4	Diode ideality factor	1.5
5	Band gap energy (eV)	1.013
6	Saturation current at reference conditions / cell (A)	1e-9
7	Short circuit current at reference conditions / cell (A)	2.5
8	Temperature coefficient of photo current (A/K)	0.001

Table 3. PV Array Parameters

1	No. of modules connected in series / array	20
2	No. of module strings in parallel / array	20
3	No. of cells connected in series / module	108
4	No. of cell strings in parallel / module	4
5	Reference irradiation (W/m^2)	607.407
6	Reference cell temperature (c°)	50

References

[1] EPIA - European Photovoltaic Industry Association "Global Market Outlook for Photovoltaic 2014-2018", 12 June 2014, Available at http://www.epia.org.

[2] Y. Yang, and F. Blaabjerg, "Low-voltage ride-through capability of a single-stage single-phase photovoltaic system connected to the low-voltage grid." *International Journal of Photo energy* 2013.

[3] A. Marinopoulos, F. Papandrea, M. Reza, S. Norrga, F. Spertino, R. Napoli, "Grid integration aspects of large solar PV installations: LVRT capability and reactive power/voltage support requirements," *Power Tech, IEEE Trondheim*, 2011 , p. 1-8.

[4] B. Xianwen, et al. "Low voltage ride through control strategy for high-power grid-connected photovoltaic inverter." *Applied Power Electronics Conference and Exposition (APEC) IEEE*, 2013.

[5] M. Mirhosseini, and V.G. Agelidis, "Performance of Large Scale Grid Connected Photovoltaic System Under Various Fault Conditions", *IEEE International Conference on Industrial Technology (ICIT), Cape Town - Australia*, 25-28 February 2013, p. 1775-1780.

[6] C-M. Lin, C-M. Young, W-S. Yeh, Y-H. Liu, "An LVRT control strategy for reducing DC-link voltage fluctuation of a two-stage photovoltaic multilevel inverter," *in Proc. Power Electronics and Drive Systems (PEDS)*, 2013, p. 908-913.

[7] H .Tian, F. Gao, and Cong Ma. "Novel low voltage ride through strategy of single-stage grid-tied photovoltaic inverter with super capacitor coupled."*Power Electronics and Motion Control Conference IEEE (IPEMC)*, Vol. 2, 2012 ,p. 1188-1192.

[8] W. Fan, et al. "Design of a Microgrid with Low-Voltage Ride-Through Capability and Simulation Experiment." *Journal of Applied Mathematics* 2014.

[9] W. Bartels, et al. "Technical Guideline Generating Plants Connected to the Medium-Voltage Network. Guideline for generating plants' connection to and parallel operation with the medium-voltage network." (2008).

[10] K. K. Weng, W. Y. Wan and R. K. Rajkumar, "Power Quality Analysis for PV Grid Connected System Using PSCAD/EMTDC." *International Journal of Renewable Energy Research (IJRER)*, Vol. 5, No. 1, 2015 ,p. 121-132.

[11] H. Muaelou, Khaled M. Abo-Al-Ez, and Ebrahim A. Badran, "Control Design of Grid-Connected PV Systems for Power Factor Correction in Distribution Power Systems Using PSCAD" *International Journal of Renewable Energy Research (IJRER)*, Vol. 6, No. 8, 2015 ,p. 1092-1099.

[12] A. Omole, "Voltage Stability Impact of Grid-Tied Photovoltaic Systems Utilizing Dynamic Reactive Power Control", *South Florida*. Ph.D. Thesis, 2010.

[13] S. Malki, "Maximum power point tracking (MPPT) for photovoltaic system." *University M'hamed Bougara Bomerdes*, M.Sc. Thesis 2011.

[14] R. Faranda and S. Leva,"Energy Comparison of MPPT Techniques for PV Systems." *WSEAS Transactions on Power Systems* , Vol. 3, No. 6, 2008, p. 446-455.

[15] Abu Tariq, M. Asim, and M. Tariq. " Simulink based modeling, simulation and Performance Evaluation of an MPPT for maximum power generation on resistive load." *2nd International Conference on Environmental Science and Technology*, Vol. 6, 2011 ,p. 397-401.

[16] A. Kalbat, "PSCAD Simulation of Grid-Tied Photovoltaic Systems and Total Harmonic Distortion Analysis",3^{rd} *International Conference on Electric Power and Energy Conversion Systems (EPECS),* Oct 2013, pp.1-6.

[17] L. Kumar, P. Kumar, and S. Ghosh, "Design of PI controller: A multiobjective optimization approach" *IEEE International Conference on Advances in Computing and Communications Informatics (ICACCI)*, 2014.

[18] R-E. Precup, S. Preitl, M-B. Rădac, E-M. Petriu, C-A. Dragoş, and J. K. Tar "*Experiment-based teaching in advanced control engineering."* IEEE Transactions on Education, Vol. 54,No. 3, 2011, pp. 345-355.

[19] K. J. Astrom "Control System Design" Lecture Note, chapter, *University of California*, 2002.

[20] Y. Yang, W. Chen, and F. Blaabjerg, " Advanced Control of Photovoltaic and Wind Turbines Power Systems " *Chapter 2 in Advanced and Intelligent Control in Power Electronics and Drives. Springer International Publishing*, pp. 41-89, 2014.